

# Transforming in-situ measurements allows robust estimation of the spatial average of soil moisture despite sensor failures

Felix Pohl<sup>1</sup>, Martin Schrön<sup>1</sup>, Corinna Rebmann<sup>2</sup>, Luis E. Samaniego<sup>3</sup>, and Anke Hildebrandt<sup>4</sup>

<sup>1</sup>Helmholtz Centre for Environmental Research GmbH - UFZ

<sup>2</sup>Helmholtz Centre for Environmental Research - UFZ

<sup>3</sup>UFZ-Helmholtz Centre for Environmental Research

<sup>4</sup>Friedrich Schiller University Jena

November 24, 2022

## Abstract

Robust estimation of average soil water content with spatial resolution of a few tens to a few hundreds of meters is essential for evaluating models or data assimilation products. Due to the high spatial variability of soil moisture at the point scale, sufficient coverage of spatial observations is required to estimate a robust field average. If sensors fail over time, averaging the remaining measurements risks the introduction of artificial shifts in the resulting time series. Here, we explore the problem of using incomplete soil moisture observations to estimate spatial averages and propose a correction accounting for temporal persistence of spatial patterns. By transforming, i.e. upscaling, each sensor measurement to the field scale using information from time periods with sufficient coverage, the dependence on full spatial coverage can be decreased. The transformed values allow to build a more robust approximation to the spatial mean, even when spatial coverage becomes sparse. We found that high temporal stability of the sensors does not necessarily guarantee that the transformed time series will provide a good estimate of the mean and therefore recommend the use of robust statistics to derive the field mean, which requires at least three estimates per observation time. The proposed protocol is applicable for observational time series with varying sample size across a given spatial extent, and it can be adopted for other variables exhibiting a temporally stable bias between the individual point observations and field scale average.

1           **Transforming in-situ measurements allows robust**  
2           **estimation of the spatial average of soil moisture**  
3           **despite sensor failures**

4           **Felix Pohl<sup>1</sup>, Martin Schrön<sup>1</sup>, Corinna Rebmann<sup>1</sup>, Luis Samaniego<sup>1</sup>, Anke**  
5           **Hildebrandt<sup>1,2,3</sup>**

6                   <sup>1</sup>Helmholtz-Centre for Environmental Research, Permoserstraße 15, 04318 Leipzig

7                   <sup>2</sup>Friedrich Schiller University Jena, Institute of Geoscience, Burgweg 11, 07749 Jena

8                   <sup>3</sup>German Centre for Integrative Biodiversity Research (iDiv) Halle-Jena-Leipzig, Puschstrasse 4, 04103  
9                   Leipzig, Germany

10           **Key Points:**

- 11           • The multi-sensor average of soil moisture data is prone to substantial bias as sen-  
12           sors fail over time.
- 13           • Reference estimates can be used to transform single sensor measurements, thus  
14           reducing the number of required sensors.
- 15           • CDF matching with dynamic piecewise linear regression can robustly transform  
16           measurements, also in the presence of extreme events.

---

Corresponding author: Felix Pohl, [felix.pohl@ufz.de](mailto:felix.pohl@ufz.de)

## Abstract

Robust estimation of average soil water content with spatial resolution of a few tens to a few hundreds of meters is essential for evaluating models or data assimilation products. Due to the high spatial variability of soil moisture at the point scale, sufficient coverage of spatial observations is required to estimate a robust field average. If sensors fail over time, averaging the remaining measurements risks the introduction of artificial shifts in the resulting time series. Here, we explore the problem of using incomplete soil moisture observations to estimate spatial averages and propose a correction accounting for temporal persistence of spatial patterns. By transforming, i.e. upscaling, each sensor measurement to the field scale using information from time periods with sufficient coverage, the dependence on full spatial coverage can be decreased. The transformed values allow to build a more robust approximation to the spatial mean, even when spatial coverage becomes sparse. We found that high temporal stability of the sensors does not necessarily guarantee that the transformed time series will provide a good estimate of the mean and therefore recommend the use of robust statistics to derive the field mean, which requires at least three estimates per observation time. The proposed protocol is applicable for observational time series with varying sample size across a given spatial extent, and it can be adopted for other variables exhibiting a temporally stable bias between the individual point observations and field scale average.

## 1 Introduction

Soil moisture is a key variable for the assessment of climate change effects on ecosystem functioning (Vereecken et al., 2008; Humphrey et al., 2018; Green et al., 2019; Humphrey et al., 2021). Although its share of the global water resources is small, soil moisture plays an essential role for maintaining transpiration, plant productivity and plant health (Jaleel et al., 2009; C. Wang et al., 2019). Especially the observation of changes in soil water balance and temporal trends are of key importance, e.g., for the further development of monitoring, early warning, and projection systems related to drought or flood events (Hao et al., 2018; Bordoni et al., 2021; Rakovec et al., 2022), for the identification of parameters in hydrological models (Cuntz et al., 2015), and for improving the parameterization of land surface models (Samaniego et al., 2017). Remote sensing products and land surface models can provide large-scale information (e.g., Babaeian et al., 2019; Yao et al., 2021), but they require robust reference data for validation and error quantification (Gruber et al., 2020).

Spatial reference estimates of soil moisture are usually derived from in-situ measurements (Gruber et al., 2020). Even modern techniques to directly measure field-average water content, such as cosmic-ray neutron sensing or remote sensing, typically require multiple in-situ measurements for calibration (Colliander et al., 2017; Schrön et al., 2017). To bridge the "support gap" between reference measurements (point scale) and target product (spatial scales from meters to kilometers) requires a transfer of the information from the lower hierarchical level to the grid scale of the target product (Y. Pachepsky & Hill, 2017). Depending on the heterogeneity of the area of interest, multiple spatial measurements are needed to estimate its spatial average soil water content reliably. Due to the strong effect of local factors on soil water dynamics, randomly located single sensor measurements are usually not representative of the entire extent (Brocca et al., 2009; Heathman et al., 2012; Zhu et al., 2018). Based on literature review, Crow et al. (2012) concluded that on an area of about 800 m<sup>2</sup> on average 10–20 sensors are required to obtain the field mean with an accuracy of 2 vol. % ( $1\sigma$ ) in the top layer. Depending on the site-specific characteristics, such as topography, vegetation or climate, the actual number of required sensors can range from 1–12 sensors (Hupet & Vanclooster, 2002) to 42 sensors (C. Wang et al., 2008) in extreme cases.

67 Even if sufficient coverage of an area is achieved by a spatial sensor setup, contin-  
68 uous monitoring is always prone to sensor failures or measurement errors (e.g., through  
69 frost, cracks or preferential flow). The corresponding gaps disrupt the integrity of the  
70 representative ensemble, which can lead to shifts, biases, and increased uncertainties in  
71 the determination of the field mean (Y. A. Pachepsky et al., 2005; Guber et al., 2008;  
72 Cosh et al., 2016). The reason is that soil moisture conditions at a given location are sub-  
73 ject to local and non-local controls (Vereecken et al., 2014; Fatichi et al., 2015; Hu et al.,  
74 2017) that can cause drier or wetter conditions on the point scale compared to the spa-  
75 tial average. Vachaud et al. (1985) demonstrated that this bias between point and field  
76 scale can be persistent in time, a phenomenon commonly referred to as temporal sta-  
77 bility (TS), or also temporal persistence, rank stability, or rank order (Chen, 2006; Van-  
78 derlinden et al., 2012). Since, numerous studies confirmed TS of soil water content (e.g.,  
79 Kachanoski & de Jong, 1988; Rolston et al., 1991) and utilized it for various hydrolog-  
80 ical applications, e.g., for data assimilation (Pan et al., 2012; Baatz et al., 2021) and model  
81 development (Brocca et al., 2017). The finding of TS was also essential for developing  
82 strategies to reduce the need for multiple spatial measurements when deriving reference  
83 values for the spatial mean. Here, TS can be used to identify locations that are repre-  
84 sentative of the area of interest (Grayson & Western, 1998; Jacobs, 2004; Brocca et al.,  
85 2009; Ran et al., 2017) or to correct the individual point-to-field scale bias when mea-  
86 suring at non-representative locations (De Lannoy et al., 2007; Crow et al., 2012; K. C. Ko-  
87 rnelsen et al., 2015)

88 In a comprehensive review on TS, Vanderlinden et al. (2012) found that 29 % of  
89 all investigated datasets had a bias in their calculation of the mean relative difference,  
90 and concluded that it was likely caused by incomplete observations. Several statistical  
91 and data-driven methods to fill missing values in soil moisture time series have been tested  
92 (Bárdossy et al., 2005; Dumedah & Coulibaly, 2011; K. Kornelsen & Coulibaly, 2014;  
93 Shao et al., 2017) ranging from fairly simple techniques such as monthly average replace-  
94 ment to more advanced approaches such as k-NN, local variance reducing techniques,  
95 artificial neural networks or evolutionary polynomial regression. While the performance  
96 of the studied methods differed, all have in common that they are only suitable for clos-  
97 ing relatively short gaps. For example, K. Kornelsen and Coulibaly (2014) recommend  
98 only filling gaps that are no longer than 72–100 hours since accuracy decreases with in-  
99 creasing gap length. Similarly, Dorigo et al. (2013) reported that the automated qual-  
100 ity control system from the International Soil Moisture Network is incapable of handling  
101 large data gaps.

102 The objective of this study is to assess a strategy to create robust spatial averages  
103 in the presence of spatially and temporally irregularly distributed data gaps. In partic-  
104 ular, we demonstrate our approach based on soil moisture data from a distributed mon-  
105 itoring network ( $\sim 1$  ha) installed in a deciduous forest in Germany, in which most of  
106 the sensors failed over time, resulting in spatial data gaps of  $> 80\%$  in comparison to  
107 the originally installed setup. Previous work has shown that only a certain number of  
108 active sensors are required to reliably estimate the spatial mean (Brocca et al., 2010; Crow  
109 et al., 2012; Gao et al., 2013; S. Lv et al., 2020), suggesting that the mean can still be  
110 estimated after sensor failure, provided enough sensors remain active. By estimating the  
111 minimum number of required sample size (MNRS), the data set can be split into refer-  
112 ence and application period. We hypothesize that a transformation of the measurements  
113 is required outside of the reference period because the temporal stability of the spatial  
114 patterns can lead to bias in the time series if sensors fail (Y. A. Pachepsky et al., 2005;  
115 Guber et al., 2008). We use the reference period to estimate parameters for the trans-  
116 formation of the remaining sensor measurements. The upscaled data can then be used  
117 to robustly approximate the spatial average, even from a small subset of the full mon-  
118 itoring network. An overview of our proposed procedure can be found in Fig. 1. Addi-  
119 tionally, we also assess the temporal stability of the sensors and discuss how it affects  
120 the accuracy of the transformation.

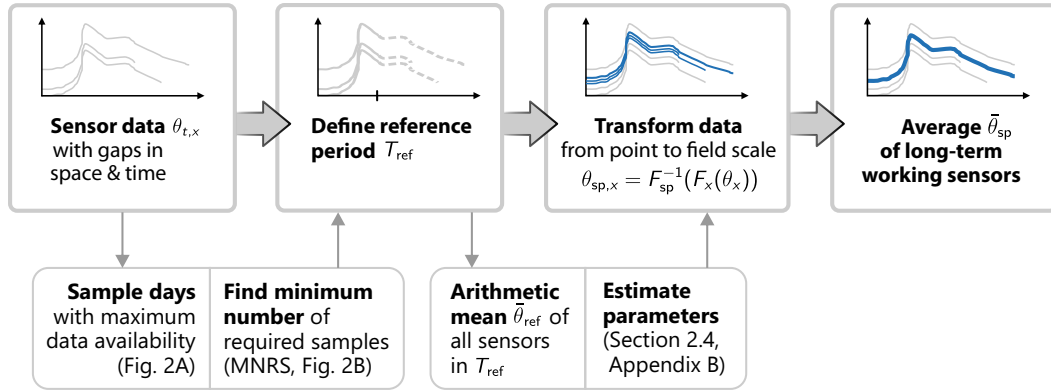


**Figure 1.** An overview of our proposed procedure to estimate the average field scale water content from in-situ measurements with gaps in space and time.

## 2 Methods and data

### 2.1 Soil moisture monitoring

Data is gathered within a 1 ha fenced area of the forest 'Hohes Holz' (DE-HoH, N52°05' E11°13', 193 m above sea-level) which is located in the northern area of the Bode water catchment near Magdeburg in Central Germany (Wollschläger et al., 2017). Soil water content sensors from a distributed monitoring network (SoilNet-WSN with SPADE sensors, sceme.de GmbH, Germany, Bogena et al., 2010) were originally installed in the frame of a trenching experiment (Marañón-Jiménez et al., 2021) in April 2014 and distributed considering patches with low and high tree (and thus root) density (21 nodes, see Fig. A1) for 15 locations. The six sensors of a node were installed in vertical profiles ranging from 10 cm to 60 cm depth. Additionally, sensors of six more nodes were distributed in the shallow layer between 10 cm and 30 cm to cover the higher soil moisture dynamics of this zone. Of the total setup described in Marañón-Jiménez et al. (2021), only sensors without soil treatment were used for our analysis. Data were acquired every 10 min via the network coordinator and stored on a field computer. In addition soil moisture was also measured with CS616 sensors (Campbell Scientific Inc., Logan, Utah, USA) in two additional profiles. Those data were also acquired and stored as 10 min averages by a CR1000 data logger (Campbell Scientific Inc., Logan, Utah, USA). More information on the research site are given in Appendix A.

Physically unrealistic data were removed by semi-automated procedures that check for limit exceedances (values below zero or above local average porosity) and spikes unrelated to precipitation. Daily averages were calculated per sensor if more than 20% of data per day was available. For the present analysis we worked with the daily averages of the period from April 2014 to April 2021. Sensors that provided data on less than 30 days were omitted to avoid low statistical power. In total, the data used here consists of measurements from 30 sensors in 10 cm, 15 sensors in 20 cm, 24 sensors in 30 cm, 16 sensors in 40 cm and 16 sensors in 50 cm. After sequential sensor failures, between 1 and 10 sensors remained in operation per layer as of 2018. We present results mainly for the 10 cm and 50 cm layers because they show the largest differences. The 60 cm layer only consisted of very few sensors in the original setup and was therefore not considered in this work.

## 152 2.2 Evaluation of temporal stability

153 Given are a number  $A$  of active measurements of volumetric soil water content,  $\theta$ ,  
 154 at locations  $x \in (1, \dots, A)$  and times  $t \in T$  during a total measurement period  $T$ . The  
 155 arithmetic spatial and temporal mean soil water contents are calculated as follows:

$$156 \quad \bar{\theta}_t = \frac{1}{A} \sum_{x \in A} \theta_{t,x} , \quad (1)$$

157 where  $\bar{\theta}_t$  is the spatial arithmetic mean over all active sensors at time  $t$  and

$$158 \quad \bar{\theta}_x = \frac{1}{T} \sum_{t \in T} \theta_{t,x} , \quad (2)$$

159 where  $\bar{\theta}_x$  is the temporal average of all observations by a sensor at location  $x$ .

160 To quantify temporal stability (TS), the mean relative difference (MRD) and its  
 161 standard deviation (SDRD) are commonly used (Vachaud et al., 1985; Vanderlinden et  
 162 al., 2012). MRD indicates the average deviation of the point measurement from the field  
 163 mean, i.e., whether a particular location is drier or wetter on average than the field mean,  
 164 and is defined as:

$$165 \quad \text{RD}_{x,t} = \frac{\theta_{x,t} - \bar{\theta}_t}{\bar{\theta}_t} , \quad (3)$$

$$166 \quad \text{MRD}_x = \frac{1}{n_x} \sum_{t=1}^{n_x} \text{RD}_{x,t} , \quad (4)$$

168 where  $\text{RD}_{x,t}$  is the relative difference of  $\theta$  at the location  $x$  and observation time  $t$ , and  
 169  $n_x$  is the number of observation days of each location. Small absolute values of  $\text{RD}_{x,t}$   
 170 indicate locations that are near the spatial average. The standard deviation of the rel-  
 171 ative difference (SDRD) can be used to describe the TS of a location, with lower values  
 172 indicating high stability or temporal persistence of the soil moisture conditions at that  
 173 location. SDRD is defined as:

$$174 \quad \text{SDRD}_x = \frac{1}{\sqrt{n_x - 1}} \sum_{t=1}^{n_x} (\text{RD}_{x,t} - \text{MRD}_x)^2 . \quad (5)$$

175 Jacobs (2004) defined a single metric that combines the information of MRD and  
 176 SDRD, that can be used to define representative locations for the target area. We fol-  
 177 low the suggestion of Zhao et al. (2010) and use the term index of time stability (ITS)  
 178 instead of RMSE proposed by Jacobs (2004) to avoid confusion with the general RMSE.  
 179 ITS can be calculated as:

$$180 \quad \text{ITS}_x = \sqrt{\text{MRD}_x^2 + \text{SDRD}_x^2} . \quad (6)$$

181 The smaller the value for ITS, the better a sensor location reflects the spatial av-  
 182 erage.

## 183 2.3 Definition of the reference period

184 We assume that the estimation error for  $\bar{\theta}_t$  is small if the sample is sufficiently large,  
 185 which implies that the identity of the sample (i.e., which sensors are active at time  $t$ )  
 186 has little effect on the estimate of  $\bar{\theta}_t$ . Obviously, due to the TS of soil moisture patterns,  
 187 with increasing sensor loss the fluctuating identity of the sample leads to different bi-  
 188 ases and increases the estimation error of  $\bar{\theta}_t$ . In order to investigate the relation between  
 189 sample size and error, for each depth we randomly selected 20 days with the largest sam-  
 190 ple size, i.e., the amount of active sensors at time  $t$ . From those, we removed randomly

191 (bootstrap with replacement,  $n = 1000$ ) some of the active sensors ( $b = 5\% \cdots 95\%$ ),  
 192 and calculated spatial averages  $\bar{\theta}_{t,b}$ . We then related the coefficient of variation of the  
 193 bootstrapped averages for each sampling stage  $b$  to the sample size. We determined the  
 194 threshold for the minimum required sample size (MNRS) based on the ratio between in-  
 195 crease in the coefficient of variation and the change in the sample size. Sample sizes at  
 196 which the increase in CV was equal to or greater than the decrease in the sample size  
 197 (Zanella et al., 2017) was used as the MNRS to estimate the spatial mean as reference.  
 198 The ensemble of all measurement intervals  $t$ , at which the amount of active sensors is  
 199 equal or greater than the estimated MNRS, forms the reference period ( $T_{\text{ref}}$ ).

## 200 2.4 Statistical transformation

201 We use a non-linear transformation to estimate the field scale average from the point  
 202 scale in situ measurements. This transformation is commonly known as "cumulative dis-  
 203 tribution function (CDF) matching" when its applied to soil moisture data (Reichle, 2004;  
 204 Drusch, 2005; De Lannoy et al., 2007; Liu et al., 2011; Han et al., 2012; S. Wang et al.,  
 205 2018) and as "quantile mapping" when it is used to correct output of climate models (Thrasher  
 206 et al., 2012; Maraun, 2013; Cannon et al., 2015). Gudmundsson et al. (2012) discuss even  
 207 more formulations that can be found in the literature. To avoid further confusion, we  
 208 will use the term "statistical transformation" as it correctly represents the technical pro-  
 209 cedure without undermining previous studies, as suggested by Gudmundsson et al. (2012).

210 We attempt to correct for the point-to-field scale bias of each sensor by finding a  
 211 function  $h$  that transforms the distribution of each sensor measurements to match the  
 212 distribution of the observed spatial average:

$$213 \theta_{\text{sp},x} = h(\theta_x) = F_{\text{sp}}^{-1}(F_x(\theta_x)), \quad (7)$$

214 where  $F$  is the CDF of the spatial (sp) and point scale soil water content, respec-  
 215 tively, and  $F^{-1}$  is the inverse CDF. We solve Eq. 7 by using the empirical CDF of the  
 216 in situ measurements and the reference spatial average ( $\bar{\theta}_{\text{ref}}$ ). Previous soil moisture re-  
 217 lated works estimated  $h$  through least square fits of a third (Drusch, 2005; De Lannoy  
 218 et al., 2007; Han et al., 2012; Gao et al., 2019; Tian et al., 2020) or fifth (Brocca et al.,  
 219 2011; Gao et al., 2017; Zhuang et al., 2020) order polynomial equation or by a 2-parametric  
 220 linear transformation (Scipal et al., 2008). Liu et al. (2009) realized the CDF matching  
 221 by dividing the CDFs into eight segments with breaks at the 5th, 10th, 25th, 50th, 75th,  
 222 90th and 95th percentile, and then applying a simple linear regression for each segment  
 223 to adjust the data. This approach has been adopted by, e.g., Liu et al. (2011) and (Xu  
 224 & Cheng, 2021) with slightly different segments.

225 We adopt piecewise linear regression (PLR) to implement CDF matching because  
 226 PLR has some advantages over polynomial models: (1) it is very flexible and therefore  
 227 allows better fits when the data to be modeled do not follow a polynomial equation, and  
 228 (2) it avoids the extrapolation problem of polynomial models since these can have strong  
 229 inflections outside the domain of the data used for matching. However, instead of using  
 230 fixed breaks for the segments, we estimated the breakpoints individually for each sen-  
 231 sor because there is no objective reason why a break in the regression model should be  
 232 expected at a certain percentile. This ensures that segments are built on breaks in the  
 233 relationship of the data and are not limited to a specific percentile.

234 Breakpoint or change point detection can be realized in various ways (van den Burg  
 235 & Williams, 2020). We used the r-package "dpseg" which offers a dynamic programming  
 236 approach by incrementally finding local optima of a score function (Machne & Stadler,  
 237 2020):

$$238 S_j = \max_{i \leq j} (S_{i-\mathcal{J}} + \text{score}(i, j)) - P \quad \text{with } \mathcal{J} \in \{0, 1\}, \quad (8)$$

where  $S$  is the  $j$ -th breakpoint,  $\mathcal{J}$  is a binary jump parameter defining whether discontinuous jumps between adjacent segments are allowed,  $P$  is a penalty parameter tuning the allowed variance per segment, and  $\text{score}(i, j)$  is a scoring function quantifying the goodness-of-fit between points  $i$  and  $j$ . The negative variance of residuals is used as the scoring function:

$$\text{score}(i, j) = -s_r^2. \quad (9)$$

Examples of the derived breakpoints and transformation functions can be found in Appendix B.

### 3 Results

#### 3.1 Minimum required sample size and temporal stability

We present spatially distributed soil moisture measurements at measurement depths of 10 cm and 50 cm. Detailed information about the particular structure of the available (respectively missing) data is given in panel A of Fig. 2. Measurements of 30 sensors in the 10 cm layer and 16 sensors in the 50 cm layer were available for our study. While some sensors delivered data for up to 98 % of the entire observation period, other sensors provided measurements only on up to 5 % of all days (or the data were rejected due to unrealistic values). Spatial data gaps are lowest at the beginning of the field study in April 2014, with most sensors failing especially during or after the winter of 2017. From 2018 on, about six to eight sensors were still operating in the 10 cm layer, while only three sensors remained in continuous operation in the 50 cm layer.

To get an idea of how the sensor failure affects the reliability of the spatial average (shown in panel A), we bootstrapped the mean of the sensors on the days with the highest data availability and then artificially reduced the sample size. The coefficient of variation (CV) of the mean is displayed in panel B in Fig. 2. The change in the CV with decreasing sensor availability shows that the CV hardly deteriorates when only a few sensors are removed, but then increases sharply when the number of sensors is small. We determined the threshold for the minimum number of required samples (MNRS) based on the ratio between increase in the coefficient of variation and the change in the sample size. The resulting MNRS is six sensors for 10 cm and five sensors for 50 cm. On these sample days with maximum data availability, the CV is less than 10 % when the MNRS is reached. It follows that the threshold ideally ensures that the CV does not exceed 10 % throughout the reference period. It also follows that in 10 cm the MNRS is given for most of the observation period, while in 50 cm only data up to 2017 can be considered as reference.

Panel C in Fig. 2 presents the rank-ordered mean relative difference (MRD), its standard deviation (SDRD) and the index of time stability (ITS) of each sensor. Note that here we have only used the previously estimated reference period with days that meet the MNRS. At each depth, sensors can be identified that are close to the average for the entire site, and likewise, some locations are much wetter or drier than average. Deviations from the mean value can range from  $-51\%$  to  $41\%$ , in relative terms. The comparison of 10 cm and 50 cm shows that the soil acts like a natural low-pass filter, causing the margins of the MRD to decrease with increasing depth. SDRD is also higher on average in the upper layer and sites with MRD close to zero can occur for both, smaller and larger SDRD, respectively.

#### 3.2 Predicting the field average from in situ measurements

By mapping the distribution of each sensor to the distribution of the spatial reference mean, the measurements of each sensor are essentially transformed into a predictor of the field mean. In other words, they are rescaled (i.e., upscaled) from the lower hierarchical level, the point scale, to the field scale. Fig. 3 presents the results of this trans-

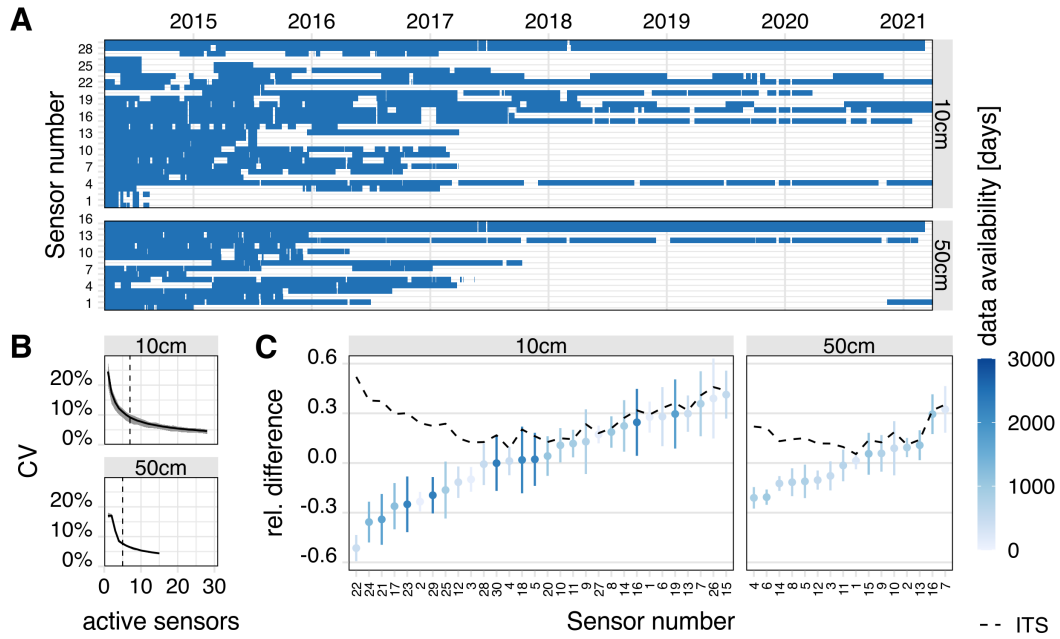


**Figure 2.** Quantitative information about the data used in this study. Panel A shows time series of data availability for two layers. Panel B shows the coefficient of variation (CV) of the bootstrapped mean soil moisture for various sample sizes at days with maximum data availability. The black line gives the average of all 20 days, and the gray area illustrates the range of CV over those days. Vertical dashed lines represent the threshold where the ratio between the change of CV and sample size becomes larger than unity, and which was taken to identify dates with sufficient data availability for a reliable estimate of the spatial average. Panel C shows the rank-ordered mean relative difference (MRD). Vertical bars are the standard deviation of the relative difference (SDRD) and the dashed line is the index of time stability (ITS). The colors refer to the number of days each sensor provided data.

288 formation. The sensors' point measurements are shown in gray and their transformed  
 289 estimates in blue colour. Panel A of Fig. 3 shows the time series of all available measure-  
 290 ments, both before and after transformation. The reference line is the arithmetic mean  
 291 of the original sensor measurements in times with sufficient data (cf. Fig. 2).

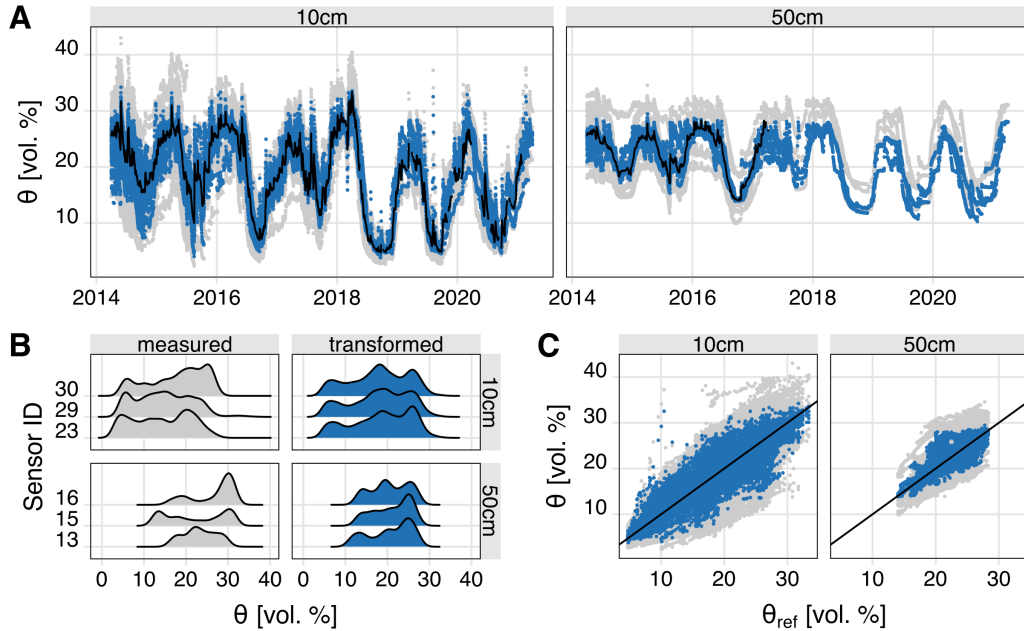


**Figure 3.** Information on the measurements in 10 cm and 50 cm before (gray) and after transformation (blue). Panel A shows the time series of all sensors, solid line is the arithmetic mean during the reference period. Panel B shows exemplarily the empirical probability density function of three sensors with most available data before (left side) and after transformation (right side). Panel C shows the scatter plot of original and transformed sensor data versus the spatial average during the reference period.

292 Panel B of Fig. 3 shows the effect of the transformation on the probability density  
 293 function (PDF) using the example of three sensors that provided most data at their re-  
 294 spective depths. Overall, the PDFs of the original sensor measurements have quite dif-  
 295 ferent shapes, with those of the sensors at 10 cm depth being much more similar than  
 296 those of the sensors at 50 cm depth. The PDFs of the sensors can be roughly summa-  
 297 rized by a bimodal shape with a peak in the wet region and a peak in the dry region,  
 298 with the exception of sensor id 13, which corresponds more to a unimodal distribution.  
 299 After transformation, the PDF of the sensors at 10 cm are very similar and follow a tri-  
 300 modal distribution with a peak in the wet region, a second peak in the intermediate re-  
 301 gion and a less pronounced third peak in the dry region. The sensors in 50 cm roughly  
 302 follow the same shape, but on a smaller range and with more variety.

303 Panel C of Fig. 3 complements the description of the transformed data with a scat-  
 304 ter plot of reference versus sensor data, both for the original measurements and the trans-  
 305 formed values. The rescaled values are much closer to the 1:1 line and less scattered than  
 306 the original measurements. In comparison of 10 cm to 50 cm, in the lower layer both the  
 307 variability and the range of the measurements is much smaller than in 10 cm. Note that  
 308 here we present the reference to the transformation based on the same reference data.  
 309 For a more detailed performance analysis with a test and training setup, the reader is  
 310 referred to Appendix C.

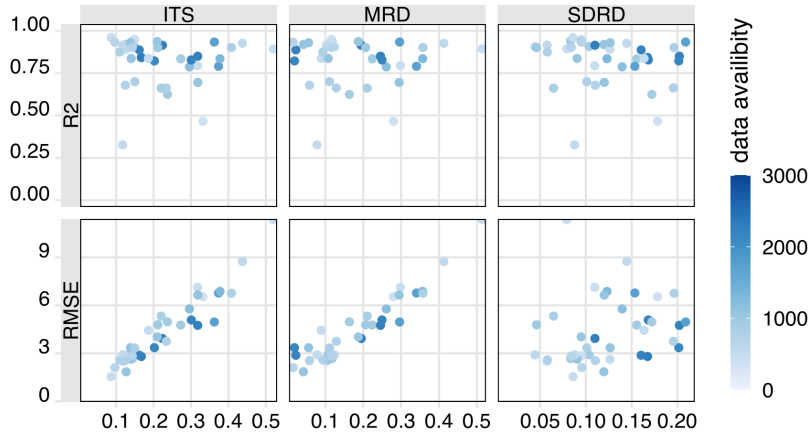


**Figure 4.** Scatter plot of  $R^2$  and RMSE of rescaled measurements versus different indicators of temporal stability. Colours refer to the amount of data of each sensor.

311 Fig. 4 shows the relationship between various methods to characterize temporal  
 312 stability (cf. Panel C, Fig. 2) and goodness of fit (gof, i.e.,  $R^2$  and RMSE) of the trans-  
 313 formed measurements during the reference period, where an estimate of the real spatial  
 314 average is available. Overall, a lower index of time stability (ITS) indicates a lower RMSE  
 315 value after transformation, while  $R^2$  remains largely unaffected. Splitting ITS into its  
 316 two components, MRD and SDRD, shows that the clear relationship between ITS and  
 317 RMSE is more dominated by MRD than SDRD.  $R^2$  appears to be largely independent  
 318 of the TS characteristics. However, it should be noted that  $R^2$  is generally high regard-  
 319 less of TS, and the only sensors with an  $R^2$  below 0.5 are those with low data availabil-  
 320 ity. In these cases, the lower goodness of fit could simply be an artifact of the short mea-  
 321 surement period.

### 322 3.3 Field average prediction with small sample sizes

323 We evaluated the effectiveness of upscaling sensors (Eq. 7) for field-scale soil wa-  
 324 ter content estimation at small sample sizes during the reference period. For this, we cal-  
 325 culated the arithmetic mean from combinations of one to six sensors (1000 repetitions)  
 326 and plot the empirical CDF of RMSE and  $R^2$  in Fig. 5. It is clear that the transfor-  
 327 mation drastically reduces the RMSE in both depth, while  $R^2$  obtained from the means of  
 328 the original measurements overall is larger than that of the transformed ones. At 10 cm,  
 329 using more than two sensors does not appreciably improve the  $R^2$  and RMSE when us-  
 330 ing the transformed data. Instead, for the original measurements, the RMSE improves  
 331 significantly with each additional sensor. The same is true for 50 cm, where the RMSE  
 332 is also overall smaller. With at least three sensors, an  $R^2$  of more than 0.8 can be ex-  
 333 pected in most cases.

334 Three sensors remained active in the 50 cm layer, and therefore the three sensors  
 335 with the highest data availability were also selected for 10 cm as a comparison. We bench-  
 336 marked the performance of the three rescaled sensors in each layer as predictors of soil  
 337 water content (Eq. 7) at the field scale against the estimate from the reference period,  
 338 and present the goodness-of-fit (gof) in Tab. 1. In addition, we also considered the use  
 339 of all three sensors and combined their estimates using the median as a robust metric  
 340 of the center of the distribution. In both depths, the  $R^2$  is higher and the RMSE lower  
 341 for the median of all compared to the individual sensors. Information on the character-  
 342 istics of TS of the sensors can also be found in Tab. 1.

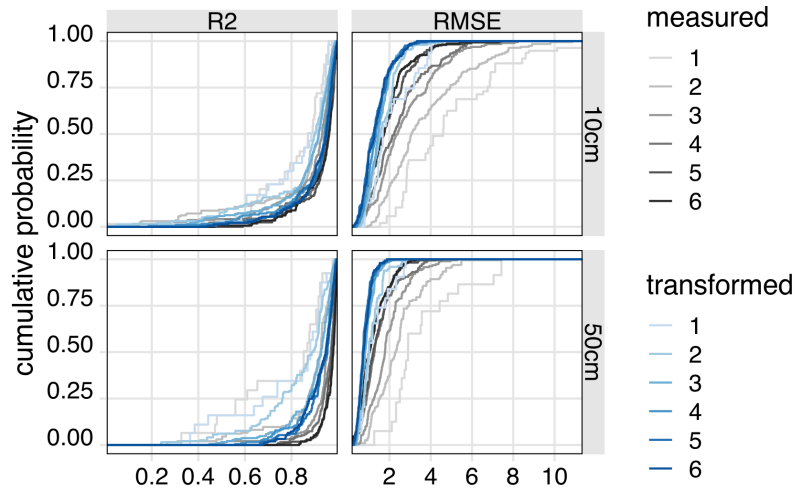


**Figure 5.** Empirical cumulative distribution function of  $R^2$  and RMSE of the relation between the reference average and the average of transformed (blue) and measured (gray) SWC for random combinations of 1–6 sensors.

**Table 1.** Example of  $R^2$  and RMSE for three sensors with most available data in both layers, and characteristics of TS for each sensor. In addition,  $R^2$  and RMSE are presented for the median of the three sensors as a robust alternative to the individual predictions of the three sensors

Depth	Predictor	$R^2$	RMSE	MRD	SDRD	ITS
10 cm	Sensor 23	0.84	2.85	0.25	0.17	0.30
	Sensor 29	0.95	1.63	0.19	0.11	0.22
	Sensor 30	0.85	2.75	0.00	0.17	0.17
	Median	0.96	1.45			
50 m	Sensor 13	0.87	1.35	0.11	0.09	0.14
	Sensor 15	0.95	0.85	0.06	0.13	0.14
	Sensor 16	0.76	1.84	0.29	0.12	0.32
	Median	0.95	0.78			

343 The estimates for the field-scale soil water content for our research site using the  
 344 transformed data is shown in Fig. 6. The difference between the simple mean of the origi-  
 345 nal data (gray line) and the median of the transformed data (orange line) illustrates the  
 346 effect of rescaling on field-scale soil water content. In winter and summer, the median  
 347 of the transformed data are about 3–4 vol. % lower than the original data. The time se-  
 348 ries shifts towards an apparently wetter regime after the reference period, likely caused  
 349 due to the sensor error than a change of the climate or soil characteristics.

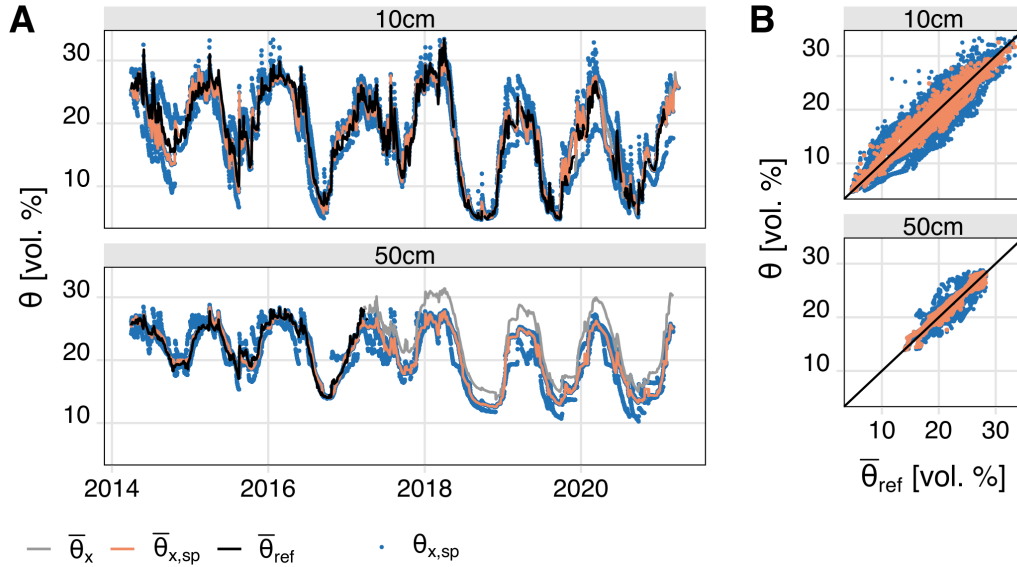


**Figure 6.** Estimated field scale soil water content in 10 cm and 50 cm. Three sensors remained working in 50 cm (cf. Panel A in Fig. 2), therefore three sensors were also selected in 10 cm (cf. Panel B in Fig. 3) based on highest data availability. Panel A shows the time series of the spatial average point estimates of the three sensors (Eq. 7,  $\theta_{x,sp}$ ) and their median  $\bar{\theta}_{x,sp}$ , respectively, the reference spatial average ( $\bar{\theta}_{ref}$ ) and the arithmetic mean of the full uncorrected dataset ( $\bar{\theta}_x$ ) outside of the reference period. Panel B shows the scatter plot of the point estimates of the three selected sensors (blue) and their median (orange), respectively, against the reference period true spatial average per layer.

## 350 4 Discussion

### 351 4.1 Challenges and limitations of working with gaps in soil moisture mea- 352 surements

353 The spatial soil moisture characteristics of the research site exhibit strong hetero-  
 354 geneity, with differences of up to 20 vol. % between sensors at the same measurement time.  
 355 The range of the mean relative difference (Panel C, Fig. 2) is comparable to results in  
 356 other studies with similar forest and climate types (L. Lv et al., 2016; Wei et al., 2017;  
 357 Zhu et al., 2021), indicating that the high degree of scatter is typically expected at such  
 358 sites. The uneven data contribution of sensors along the dry-humid gradient within the  
 359 data set creates a systematic problem when the remaining measurements of incomplete  
 360 measurements are averaged: Due to the ordered structure of the data, a changing num-  
 361 ber of active sensors can lead to a systematic bias of the time series at the field scale (Y. A. Pachep-  
 362 sky et al., 2005; Guber et al., 2008). For example, if more sensors fail in drier locations,  
 363 a time series of calculated spatial average using Eq. 1 would gradually shift more toward

364 the wetter environment and thus does not reflect the entire study site anymore. This be-  
365 havior was observed in the 50 cm layer (see Fig. 6). After the failure of most sensors in  
366 2017, an artificial shift towards a wetter regime was observed.

367 In principle, it is always desirable to have complete measurement series, but data  
368 failure is not uncommon in field studies. However, the bootstrapping simulation shows  
369 that as long as a minimum number of sensors is active, the estimation uncertainty of the  
370 spatial mean is negligible. Bootstrapping is a robust method to estimate the sampling  
371 distribution if the true distribution is unknown, and therefore also commonly used to as-  
372 sess the statistical distribution of soil moisture measurements (Rowlandson et al., 2015;  
373 Singh et al., 2019; Fatholouloumi et al., 2021). C. Wang et al. (2008) compared bootstrap-  
374 based estimation of required sample size with other geo-statistical and stratified sam-  
375 pling strategies and found similar results among the methods. Due to limited data avail-  
376 ability, we only examined exemplary days with the greatest possible completeness. It is  
377 known that the spatial variability of soil water content changes with different phases (wet-  
378 ting, drying) (Illston et al., 2004; Vereecken et al., 2014), absolute water content (Brocca  
379 et al., 2010; Peng et al., 2016) and phenological state of the ecosystem (T. Wang et al.,  
380 2015). Therefore, in future studies, it might be advisable with better data availability  
381 to investigate MNRS separately for different phases. Because there may be seasonal con-  
382 trols and seasonal variation of the spatial dispersion (Hupet & Vanclooster, 2002; Illston  
383 et al., 2004; Biswas, 2014; Hu et al., 2017), predictions could be improved by estimat-  
384 ing seasonal correction functions. However, this procedure might lead to jumps in the  
385 time series when moving from one season to the next, and was therefore not considered  
386 in this study.

387 The estimated threshold value of the MNRS for a reliable averaging of the mea-  
388 sured values showed that only in the 10 cm layer sufficient sensors were consistently ac-  
389 tive (with the exception of a few days). In the other depths the threshold value was un-  
390 dercut, so that the derivation of an average without correction would lead to a biased  
391 time series. Especially obvious in 50 cm depth, a clear difference between measured and  
392 transformed data can be seen outside the reference period. Although a definitive assess-  
393 ment of goodness-of-fit in later years is not possible for our remaining measurements due  
394 to the lack of reference values, it shows how increasing bias threatens to manifest itself  
395 as a temporal trend. Furthermore, the proposed corrected time series is clearly a bet-  
396 ter estimate of the true spatial average for the following two reasons: First, the sudden  
397 increase in soil moisture in winter should be explainable by physical reasons by major  
398 changes in climatic conditions, since soil moisture was at a similar level in all previous  
399 winters. In fact, however, an extreme drought began in Central Europe in the summer  
400 of 2018, which also affected the study region. A daily time series of the Standardized Pre-  
401 cipitation Evapotranspiration Index for a nearby research site can be found in Hermanns  
402 et al. (2021). Thus, an apparent shift toward a wetter regime is implausible.

403 Second, the measurements of the 10 cm layer can be used as a surrogate for a ref-  
404 erence, since enough sensors were active during the entire study period. Although the  
405 soil acts as a low-pass filter, resulting in much less diurnal variability in the deeper soil  
406 layer than in the higher layers, there should still be a clear statistical relationship be-  
407 tween the spatial averages between the corresponding depths. Correlating the time se-  
408 ries of the spatial mean during the reference period (e.g. the best estimate of the true  
409 spatial mean) in 10 cm (cf. Fig. 5) with the field scale average time series in 50 cm yields  
410 an  $R^2$  of 0.74 for the original measurements and 0.89 for the transformed measurements  
411 (not shown). Likewise, the RMSE decreases from 5.77 % for the original measurements  
412 to 4.06 % for the transformed measurements (not shown). Both statistics indicate a stronger  
413 relationship between layers when the transformed average is used in 50 cm.

## 414 4.2 Robust estimates of spatial soil moisture averages

415 The proposed statistical transformation is technically equivalent to other upscal-  
 416 ing studies and several transformation approaches have been discussed in the literature,  
 417 ranging from simple linear scaling (De Lannoy et al., 2007; Crow et al., 2012) to more  
 418 advanced approaches such as Bayesian regression (Qin et al., 2013), block kriging (J. Wang  
 419 et al., 2015), random forest (Clewley et al., 2017; Zappa et al., 2019) or deep learning  
 420 methods (Zhang et al., 2017). For an extensive comparison of nonlinear rescaling func-  
 421 tions see Afshar and Yilmaz (2017). Since many of these techniques involve rescaling of  
 422 remote sensing products, the applicability of their results to upscaling of in situ mea-  
 423 surements of individual sites needs to be examined.

424 To save cost and effort, it is generally desirable to measure at single points rather  
 425 than with multiple, randomly distributed measurements. Many studies have investigated  
 426 the feasibility to utilize TS of spatial patterns to use representative measurement loca-  
 427 tions (RML) for the spatial average (e.g., Rivera et al., 2014; Molero et al., 2018; Singh  
 428 et al., 2019; Fry & Guber, 2020). On the other hand, there are studies that report that  
 429 TS can change inter-seasonally (Zhao et al., 2010; Biswas, 2014; Dari et al., 2019) or that  
 430 TS could not be confirmed depending on the type of measurement (Kirda & Reichardt,  
 431 2000; Heathman et al., 2012; Vanderlinden et al., 2012). Likewise, we found that with  
 432 our data no single sensor could perfectly replace the reference measurements and that  
 433 characteristics of temporal stability were only partly related to the accuracy of the rescaled  
 434 measurements. We therefore deduce that, for deriving spatial averages from small sam-  
 435 ples, it is more reliable to use all available measurements and combine them by using ro-  
 436 bust estimates for the statistical location (Rousseeuw & Verboven, 2002) instead of work-  
 437 ing with single representative, potentially upscaled sensors.

## 438 5 Conclusions

439 In this study, we used a data set of continuous soil moisture measurements over seven  
 440 years at a deciduous forest site with a large number of consecutive sensor failures to il-  
 441 lustrate the problem of averaging incomplete observations. The characteristics of the tem-  
 442 poral stability are comparable to other studies with similar forest and climate types. We  
 443 found that as the number of sensor failures increases, the risk and magnitude of artifi-  
 444 cial shifts in the time series of the field mean increase due to the large spatial hetero-  
 445 geneity of soil moisture. Therefore, we adopted a strategy to cope with the spatial data  
 446 gaps and temporally inconsistent sensor failures. First, we estimated the number of min-  
 447 imum required spatial sensor coverage to determine reference values for the spatial mean.  
 448 In the second step, we corrected the point-to-field scale bias of the remaining sensor mea-  
 449 surements outside the reference period. The corrected measurements could then be used  
 450 to reliably determine the spatial mean despite extensive spatial data gaps. To estimate  
 451 the spatial average from the upscaled data, we found that the median of the remaining  
 452 measurements yields a higher accuracy rather than using single locations as represen-  
 453 tatives.

454 Overall, we emphasize the importance of making adequate adjustments for failed  
 455 sensors when averaging spatial in situ measurements. Systematic spatial bias can intro-  
 456 duce artificial trends in the spatial average time series that would affect interpretations  
 457 regarding extreme events or regime shifts due to anthropogenic change. The results of  
 458 this study can also be applied to other research areas where a temporally stable bias be-  
 459 tween point and spatial estimates can be expected. Furthermore, the results may be use-  
 460 ful not only in the context of sensor failures, but also in reducing measurement effort.  
 461 Once the spatial mean can be reliably estimated from a small number of sensors, it is  
 462 possible to operate the network with a reduced setup. At the same time, the transfor-  
 463 mation of the measurements requires reference estimates, and so far too little is known  
 464 about how long and to what extent these reference measurements have to be operated.

465 Future research should focus on sensitivity to the length and spatial scale of those ref-  
466 erence estimates. At the same time, indirect measurements from remote sensing prod-  
467 ucts as well as cosmic-ray neutron sensing measurements could be useful sources of in-  
468 formation to further reduce the in situ effort required for reference determinations of soil  
469 water content.

470 **Appendix A Research site description**

471 The 'Hohes Holz' is a deciduous forest covering an area of around 15 km<sup>2</sup>, domi-  
 472 nated by sessile oak (*Quercus petraea* (Matt.) Liebl.), common beech (*Fagus sylvatica*  
 473 L.), and hornbeam (*Carpinus betulus* L.). The climate is a temperate climate with a mean  
 474 annual temperature of 9.1 °C and a mean annual precipitation of 563 mm (climate pe-  
 475 riod 1981–2010, station Ummendorf of the German Weather Service). During the inves-  
 476 tigated period from 2014 until 2020 yearly precipitation sums ranged from 301 mm (2018)  
 477 to 610 mm (2017). The bedrock is Pleistocene sandy loess above till and Mesozoic muschel-  
 478 kalk, with Haplic Cambisol as predominant soil type. Soil texture at 0–20 cm depth was  
 479 3.0 % ( $\pm 1.8\%$ ) sand, 87.1 % ( $\pm 2.1\%$ ) silt, and 10.0 % ( $\pm 2.2\%$ ) clay.

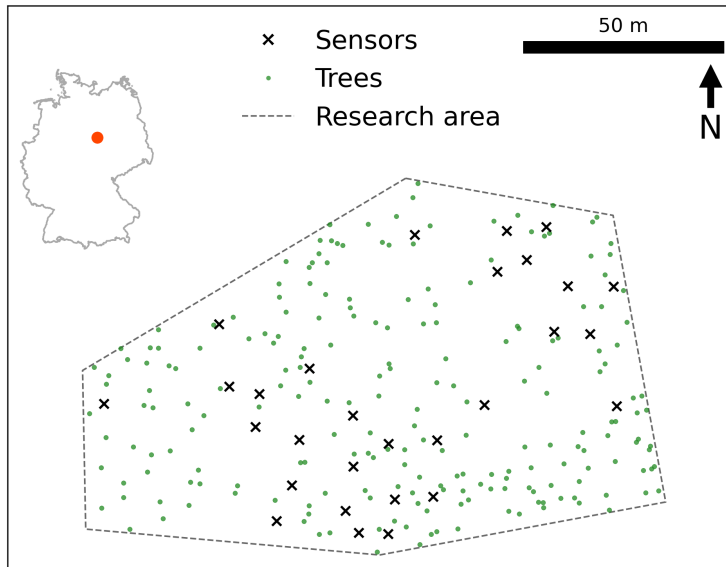


**Figure A1.** Sensor distribution in the study area 'Hohes Holz' (DE-HoH) with additional information on tree density and the location of the study area in Germany. Note that at each marker sensors are distributed over the depths from 10 cm to 60 cm in 10 cm intervals, but not all depths are covered at each marker.

480

**Appendix B CDF matching with dynamic piecewise linear regression**

481

482

483

484

485

486

487

488

489

We compare polynomial fits, which are traditionally used for cumulative distribution function (CDF) matching, against the piecewise linear regression (PLR) approach with flexible segments, proposed in this study. Fig. B1 shows exemplary the difference between the spatial reference mean and sensors with most available data. Sensor 16 in 50 cm and sensor 23 in 10 cm are good examples of how the polynomial fit can lead to large over- or underestimates, especially in the context of extrapolation. The PLR approach can theoretically be fit to any functional form and extrapolation can be realized by adopting the last known linear function at the minimum and maximum spatial reference.

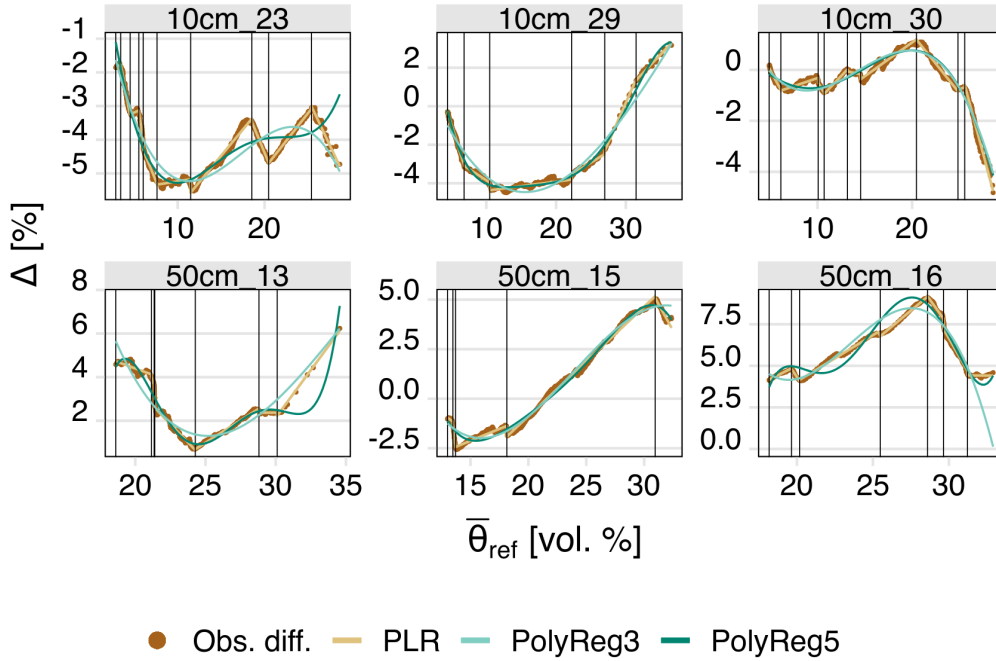


**Figure B1.** Transformation functions for exemplary sensors with the most available data (see Fig. 2). The dots are the observed difference between the CDFs and the lines are the derived functions for fitting the CDF of the sensors to the CDF of the spatial reference mean. CDFs before and after transformation are shown in Fig. 3. In this study, dynamic piecewise linear regression was used (PLR); for comparison, the traditionally used fits with polynomial regression (third and fifth order, respectively) are also shown. Vertical lines are the breaks of the PLR.

490 **Appendix C Performance of statistical transformation**

491 Similar to De Lannoy et al. (2007) and Gudmundsson et al. (2012), we benchmarked  
 492 the proposed transformation of section 2.4 against the following parametric transforma-  
 493 tions:

$$\theta_{\text{sp},x} = a + \theta_x \quad (\text{C1})$$

$$\theta_{\text{sp},x} = b \cdot \theta_x \quad (\text{C2})$$

$$\theta_{\text{sp},x} = a + b \cdot \theta_x \quad (\text{C3})$$

494 where  $\theta$  is the soil moisture on the point and field scale, respectively, and  $a, b$  are param-  
 495 eters to be estimated. We split the data of the reference period into two equally sized  
 496 groups to test the performance of the transformations. The parameters of the scaling  
 497 methods were estimated using the training data and then applied to the test data. The  
 498 accuracy of the fit between the observed and estimated field average soil moisture was  
 499 assessed with the following goodness-of-fit parameters: Mean absolute error (MAE), Root  
 500 Mean Square Error (RMSE), Pearson correlation coefficient (R) and Nash-Sutcliffe ef-  
 501 ficiency (NS):

$$\text{MAE} = |\bar{y} - \bar{\hat{y}}| \quad (\text{C4})$$

$$\text{RMSE} = \sqrt{\frac{1}{N} \sum_{i=1}^N (y_i - \hat{y}_i)^2} \quad (\text{C5})$$

$$\text{R} = \frac{\text{Cov}(y, \hat{y})}{s_y s_{\hat{y}}} \quad (\text{C6})$$

$$\text{NS} = 1 - \frac{\sum_{i=1}^N (y_i - \hat{y}_i)^2}{\sum_{i=1}^N (y_i - \bar{y})^2}. \quad (\text{C7})$$

502 Tab. C1 summarizes the results for each method as the mean of the gof of all sens-  
 503 ors per layer. In every layer and with every gof, the non-linear CDF matching achieved  
 504 best results. Among the linear methods, the linear regression usually performed best.  
 505 Both, the MAE and RMSE decrease with depth, with a maximum MAE of 2.76 % for  
 506  $\theta_{\text{C2}}$  in 30 cm and a minimum of 1.02 % for  $\theta_{\text{CDF}}$  in 50 cm. The correlation coefficient shows  
 507 narrow ranges per layer, with very strong correlations for all  $m\theta_{\text{CDF}}$  in 40 cm (0.94) and  
 508 lowest correlation for  $\theta_{\text{C1}}$  in 50 cm (0.85). The Nash-Sutcliffe model efficiency coefficient  
 509 (NS) shows lowest performance in 50 cm (0.712 for  $\theta_{\text{C1}}$ ) and highest performance in 10 cm  
 510 (0.87 for  $\theta_{\text{CDF}}$ ). RMSE is lowest for  $\theta_{\text{C3}}$  (1.50 % in 50 cm) and highest for  $\theta_{\text{C2}}$  (3.66 %  
 511 in 30 cm).

**Table C1.** Mean average error (MAE, [vol. %]), Nash-Sutcliffe criterium (NS, [-]), correla-  
 tion coefficient (R, [-]) and root mean square error (RMSE, [vol. %]) between the spatial average  
 soil moisture and transformed point measurements during the reference period. Scores are the  
 average over all sensors per layer.

Layer	MAE				NS				R				RMSE			
	$\theta_{\text{C1}}$	$\theta_{\text{C2}}$	$\theta_{\text{C3}}$	$\theta_{\text{CDF}}$												
10 cm	2.03	2.15	1.88	1.75	0.84	0.84	0.84	0.87	0.92	0.91	0.93	0.93	2.69	2.87	2.43	2.41
20 cm	1.89	2.22	1.58	1.32	0.80	0.77	0.80	0.85	0.89	0.88	0.91	0.93	2.45	2.82	2.01	1.89
30 cm	2.02	2.76	1.70	1.51	0.80	0.74	0.80	0.84	0.90	0.87	0.91	0.92	2.79	3.66	2.26	2.22
40 cm	1.77	1.92	1.48	1.24	0.84	0.83	0.86	0.88	0.92	0.91	0.93	0.94	2.34	2.45	1.91	1.85
50 cm	1.56	1.54	1.11	1.02	0.72	0.74	0.75	0.80	0.85	0.86	0.90	0.90	2.07	2.00	1.50	1.51

## Appendix D Open Research

The daily averaged soil moisture measurements used in the study are available at the Helmholtz-Centre for Environmental Research data archive via doi.org/10.48758/ufz.12770 under CC BY-NC-SA 4.0 (Rebmann et al., 2018). The code to reproduce all results and figures (except for Fig. 1 and Fig. A1) is preserved at doi.org/10.5281/zenodo.6653168 and available under CC BY-NC-SA 4.0 (Pohl et al., 2022).

### Acknowledgments

A.H. gratefully acknowledges the support of iDiv funded by the German Research Foundation (DFG– FZT 118, 202548816) and CRC AquaDiva (SFB 1076 – Project Number 218627073). M.S. acknowledges support by the DFG (German Research Foundation) via the project 357874777, research unit FOR 2694 Cosmic Sense. The study has been made possible by the infrastructural funds of the Helmholtz Association and the Terrestrial Environmental Observatories (TERENO). The operation and data gathering of field data was supported by Sebastian Gimper and Patrick Schmidt. Juliane Mai and Matthias Cuntz supported the data-treatment procedures in previous versions. We thank Floris Hermanns for his support in Fig. A1.

### References

- Afshar, M., & Yilmaz, M. (2017). The added utility of nonlinear methods compared to linear methods in rescaling soil moisture products. *Remote Sensing of Environment*, *196*, 224–237. doi: 10.1016/j.rse.2017.05.017
- Baatz, R., Hendricks Franssen, H. J., Euskirchen, E., Sihi, D., Dietze, M., Ciavatta, S., ... Vereecken, H. (2021). Reanalysis in Earth System Science: Toward Terrestrial Ecosystem Reanalysis. *Reviews of Geophysics*, *59*(3). doi: 10.1029/2020RG000715
- Babaeian, E., Sadeghi, M., Jones, S. B., Montzka, C., Vereecken, H., & Tuller, M. (2019). Ground, Proximal, and Satellite Remote Sensing of Soil Moisture. *Reviews of Geophysics*, *57*(2), 530–616. doi: 10.1029/2018RG000618
- Bárdossy, A., Pegram, G. G. S., & Samaniego, L. (2005). Modeling data relationships with a local variance reducing technique: Applications in hydrology. *Water Resources Research*, *41*(8). doi: 10.1029/2004WR003851
- Biswas, A. (2014). Season- and depth-dependent time stability for characterising representative monitoring locations of soil water storage in a hummocky landscape. *CATENA*, *116*, 38–50. doi: 10.1016/j.catena.2013.12.008
- Bogena, H., Herbst, M., Huisman, J., Rosenbaum, U., Weuthen, A., & Vereecken, H. (2010). Potential of Wireless Sensor Networks for Measuring Soil Water Content Variability. *Vadose Zone Journal*, *9*(4), 1002–1013. doi: 10.2136/vzj2009.0173
- Bordoni, M., Inzaghi, F., Vivaldi, V., Valentino, R., Bittelli, M., & Meisina, C. (2021). A Data-Driven Method for the Temporal Estimation of Soil Water Potential and Its Application for Shallow Landslides Prediction. *Water*, *13*(9), 1208. doi: 10.3390/w13091208
- Brocca, L., Ciabatta, L., Massari, C., Camici, S., & Tarpanelli, A. (2017). Soil Moisture for Hydrological Applications: Open Questions and New Opportunities. *Water*, *9*(2), 140. doi: 10.3390/w9020140
- Brocca, L., Hasenauer, S., Lacava, T., Melone, F., Moramarco, T., Wagner, W., ... Bittelli, M. (2011). Soil moisture estimation through ASCAT and AMSR-E sensors: An intercomparison and validation study across Europe. *Remote Sensing of Environment*, *115*(12), 3390–3408. doi: 10.1016/j.rse.2011.08.003
- Brocca, L., Melone, F., Moramarco, T., & Morbidelli, R. (2009). Soil moisture temporal stability over experimental areas in Central Italy. *Geoderma*, *148*(3-4), 364–374. doi: 10.1016/j.geoderma.2008.11.004

- 563 Brocca, L., Melone, F., Moramarco, T., & Morbidelli, R. (2010). Spatial-temporal  
564 variability of soil moisture and its estimation across scales. *Water Resources*  
565 *Research*, *46*(2). doi: 10.1029/2009WR008016
- 566 Cannon, A. J., Sobie, S. R., & Murdock, T. Q. (2015). Bias Correction of GCM  
567 Precipitation by Quantile Mapping: How Well Do Methods Preserve Changes  
568 in Quantiles and Extremes? *Journal of Climate*, *28*(17), 6938–6959. doi:  
569 10.1175/JCLI-D-14-00754.1
- 570 Chen, Y.-j. (2006). Letter to the Editor on “Rank Stability or Temporal Stabil-  
571 ity”. *Soil Science Society of America Journal*, *70*(1), 306–306. doi: 10.2136/  
572 sssaj2005.0290l
- 573 Clewley, D., Whitcomb, J. B., Akbar, R., Silva, A. R., Berg, A., Adams, J. R., ...  
574 Moghaddam, M. (2017). A Method for Upscaling In Situ Soil Moisture Mea-  
575 surements to Satellite Footprint Scale Using Random Forests. *IEEE Journal*  
576 *of Selected Topics in Applied Earth Observations and Remote Sensing*, *10*(6),  
577 2663–2673. doi: 10.1109/JSTARS.2017.2690220
- 578 Colliander, A., Jackson, T., Bindlish, R., Chan, S., Das, N., Kim, S., ... Yueh,  
579 S. (2017). Validation of SMAP surface soil moisture products with core  
580 validation sites. *Remote Sensing of Environment*, *191*, 215–231. doi:  
581 10.1016/j.rse.2017.01.021
- 582 Cosh, M. H., Ochsner, T. E., McKee, L., Dong, J., Basara, J. B., Evett, S. R., ...  
583 Sayde, C. (2016). The Soil Moisture Active Passive Marena, Oklahoma, In Situ  
584 Sensor Testbed (SMAP-MOISST): Testbed Design and Evaluation of In Situ  
585 Sensors. *Vadose Zone Journal*, *15*(4), 1–11. doi: 10.2136/vzj2015.09.0122
- 586 Crow, W. T., Berg, A. A., Cosh, M. H., Loew, A., Mohanty, B. P., Panciera, R., ...  
587 Walker, J. P. (2012). Upscaling sparse ground-based soil moisture observations  
588 for the validation of coarse-resolution satellite soil moisture products. *Reviews*  
589 *of Geophysics*, *50*(2). doi: 10.1029/2011RG000372
- 590 Cuntz, M., Mai, J., Zink, M., Thober, S., Kumar, R., Schäfer, D., ... Samaniego,  
591 L. (2015). Computationally inexpensive identification of noninformative  
592 model parameters by sequential screening. *Water Resources Research*, *51*(8),  
593 6417–6441. doi: 10.1002/2015WR016907
- 594 Dari, J., Morbidelli, R., Saltalippi, C., Massari, C., & Brocca, L. (2019). Spatial-  
595 temporal variability of soil moisture: Addressing the monitoring at the  
596 catchment scale. *Journal of Hydrology*, *570*, 436–444. doi: 10.1016/  
597 j.jhydrol.2019.01.014
- 598 De Lannoy, G. J., Houser, P. R., Verhoest, N. E., Pauwels, V. R., & Gish, T. J.  
599 (2007). Upscaling of point soil moisture measurements to field aver-  
600 ages at the OPE3 test site. *Journal of Hydrology*, *343*(1-2), 1–11. doi:  
601 10.1016/j.jhydrol.2007.06.004
- 602 Dorigo, W., Xaver, A., Vreugdenhil, M., Gruber, A., Hegyiová, A., Sanchis-Dufau,  
603 A., ... Drusch, M. (2013). Global Automated Quality Control of In Situ Soil  
604 Moisture Data from the International Soil Moisture Network. *Vadose Zone*  
605 *Journal*, *12*(3), vzj2012.0097. doi: 10.2136/vzj2012.0097
- 606 Drusch, M. (2005). Observation operators for the direct assimilation of TRMM mi-  
607 crowave imager retrieved soil moisture. *Geophysical Research Letters*, *32*(15),  
608 L15403. doi: 10.1029/2005GL023623
- 609 Dumedah, G., & Coulibaly, P. (2011). Evaluation of statistical methods for infill-  
610 ing missing values in high-resolution soil moisture data. *Journal of Hydrology*,  
611 *400*(1-2), 95–102. doi: 10.1016/j.jhydrol.2011.01.028
- 612 Fatholouloumi, S., Vaezi, A. R., Firozjaei, M. K., & Biswas, A. (2021). Quan-  
613 tifying the effect of surface heterogeneity on soil moisture across regions  
614 and surface characteristic. *Journal of Hydrology*, *596*, 126132. doi:  
615 10.1016/j.jhydrol.2021.126132
- 616 Fatichi, S., Katul, G. G., Ivanov, V. Y., Pappas, C., Paschalis, A., Consolo, A., ...  
617 Burlando, P. (2015). Abiotic and biotic controls of soil moisture spatiotem-

- 618 poral variability and the occurrence of hysteresis. *Water Resources Research*,  
619 51(5), 3505–3524. doi: 10.1002/2014WR016102
- 620 Fry, J. E., & Guber, A. K. (2020). Temporal stability of field-scale patterns in soil  
621 water content across topographically diverse agricultural landscapes. *Journal*  
622 *of Hydrology*, 580, 124260. doi: 10.1016/j.jhydrol.2019.124260
- 623 Gao, X., Wu, P., Zhao, X., Wang, J., Shi, Y., Zhang, B., . . . Li, H. (2013). Estima-  
624 tion of spatial soil moisture averages in a large gully of the Loess Plateau of  
625 China through statistical and modeling solutions. *Journal of Hydrology*, 486,  
626 466–478. doi: 10.1016/j.jhydrol.2013.02.026
- 627 Gao, X., Zhao, X., Brocca, L., Huo, G., Lv, T., & Wu, P. (2017). *Depth scaling of*  
628 *soil moisture content from surface to profile: Multistation testing of observation*  
629 *operators* (Preprint). Vadose Zone Hydrology/Modelling approaches. doi:  
630 10.5194/hess-2017-292
- 631 Gao, X., Zhao, X., Brocca, L., Pan, D., & Wu, P. (2019). Testing of observation  
632 operators designed to estimate profile soil moisture from surface measurements.  
633 *Hydrological Processes*, 33(4), 575–584. doi: 10.1002/hyp.13344
- 634 Grayson, R. B., & Western, A. W. (1998). Towards areal estimation of soil water  
635 content from point measurements: Time and space stability of mean response.  
636 *Water Resources Research*, 207(1/2), 15.
- 637 Green, J. K., Seneviratne, S. I., Berg, A. M., Findell, K. L., Hagemann, S.,  
638 Lawrence, D. M., & Gentine, P. (2019). Large influence of soil moisture  
639 on long-term terrestrial carbon uptake. *Nature*, 565(7740), 476–479. doi:  
640 10.1038/s41586-018-0848-x
- 641 Gruber, A., De Lannoy, G., Albergel, C., Al-Yaari, A., Brocca, L., Calvet, J.-C., . . .  
642 Wagner, W. (2020). Validation practices for satellite soil moisture retrievals:  
643 What are (the) errors? *Remote Sensing of Environment*, 244, 111806. doi:  
644 10.1016/j.rse.2020.111806
- 645 Guber, A., Gish, T., Pachepsky, Y., van Genuchten, M., Daughtry, C., Nichol-  
646 son, T., & Cady, R. (2008). Temporal stability in soil water content  
647 patterns across agricultural fields. *CATENA*, 73(1), 125–133. doi:  
648 10.1016/j.catena.2007.09.010
- 649 Gudmundsson, L., Bremnes, J. B., Haugen, J. E., & Engen-Skaugen, T. (2012).  
650 Technical Note: Downscaling RCM precipitation to the station scale using  
651 statistical transformations – a comparison of methods. *Hydrology and Earth*  
652 *System Sciences*, 16(9), 3383–3390. doi: 10.5194/hess-16-3383-2012
- 653 Han, E., Heathman, G. C., Merwade, V., & Cosh, M. H. (2012). Application  
654 of observation operators for field scale soil moisture averages and variances  
655 in agricultural landscapes. *Journal of Hydrology*, 444–445, 34–50. doi:  
656 10.1016/j.jhydrol.2012.03.035
- 657 Hao, Z., Singh, V. P., & Xia, Y. (2018). Seasonal Drought Prediction: Advances,  
658 Challenges, and Future Prospects. *Reviews of Geophysics*, 56(1), 108–141. doi:  
659 10.1002/2016RG000549
- 660 Heathman, G. C., Cosh, M. H., Han, E., Jackson, T. J., McKee, L., & McAfee,  
661 S. (2012). Field scale spatiotemporal analysis of surface soil moisture  
662 for evaluating point-scale in situ networks. *Geoderma*, 170, 195–205. doi:  
663 10.1016/j.geoderma.2011.11.004
- 664 Hermanns, F., Pohl, F., Rebmann, C., Schulz, G., Werban, U., & Lausch, A. (2021).  
665 Inferring Grassland Drought Stress with Unsupervised Learning from Air-  
666 borne Hyperspectral VNIR Imagery. *Remote Sensing*, 13(10), 1885. doi:  
667 10.3390/rs13101885
- 668 Hu, W., Si, B. C., Biswas, A., & Chau, H. W. (2017). Temporally stable patterns  
669 but seasonal dependent controls of soil water content: Evidence from wavelet  
670 analyses. *Hydrological Processes*, 31(21), 3697–3707. doi: 10.1002/hyp.11289
- 671 Humphrey, V., Berg, A., Ciais, P., Gentine, P., Jung, M., Reichstein, M., . . .  
672 Frankenberg, C. (2021). Soil moisture–atmosphere feedback domi-

- 673 nates land carbon uptake variability. *Nature*, 592(7852), 65–69. doi:  
674 10.1038/s41586-021-03325-5
- 675 Humphrey, V., Zscheischler, J., Ciais, P., Gudmundsson, L., Sitch, S., & Senevi-  
676 ratne, S. I. (2018). Sensitivity of atmospheric CO<sub>2</sub> growth rate to ob-  
677 served changes in terrestrial water storage. *Nature*, 560(7720), 628–631.  
678 doi: 10.1038/s41586-018-0424-4
- 679 Hupet, F., & Vanclooster, M. (2002). Intraseasonal dynamics of soil moisture vari-  
680 ability within a small agricultural maize cropped field. *Journal of Hydrology*,  
681 16.
- 682 Illston, B. G., Basara, J. B., & Crawford, K. C. (2004). Seasonal to interannual vari-  
683 ations of soil moisture measured in Oklahoma. *Int. J. Climatol.*, 14.
- 684 Jacobs, J. (2004). SMEX02: Field scale variability, time stability and similarity of  
685 soil moisture. *Remote Sensing of Environment*, 92(4), 436–446. doi: 10.1016/  
686 j.rse.2004.02.017
- 687 Jaleel, C. A., Manivannan, P., Wahid, A., Farooq, M., Al-Juburi, J., Somasundaram,  
688 R., & Panneerselvam, R. (2009). Drought Stress in Plants: A Review on  
689 Morphological Characteristics and Pigments Composition. *Int. J. Agric. Biol.*,  
690 11(1), 6.
- 691 Kachanoski, R. G., & de Jong, E. (1988). Scale dependence and the temporal per-  
692 sistence of spatial patterns of soil water storage. *Water Resources Research*,  
693 24(1), 85–91. doi: 10.1029/WR024i001p00085
- 694 Kirda, C., & Reichardt, K. (2000). Comparison of neutron moisture gauges with  
695 non-nuclear methods to measure field soil water status. *International Agro-*  
696 *physics*, 6(1-2), 77–87.
- 697 Kornelsen, K., & Coulibaly, P. (2014). Comparison of Interpolation, Statistical,  
698 and Data-Driven Methods for Imputation of Missing Values in a Distributed  
699 Soil Moisture Dataset. *Journal of Hydrologic Engineering*, 19(1), 26–43. doi:  
700 10.1061/(ASCE)HE.1943-5584.0000767
- 701 Kornelsen, K. C., Cosh, M. H., & Coulibaly, P. (2015). Potential of bias correction  
702 for downscaling passive microwave and soil moisture data: Bias Correction  
703 Downscaling. *Journal of Geophysical Research: Atmospheres*, 120(13), 6460–  
704 6479. doi: 10.1002/2015JD023550
- 705 Liu, Y. Y., Parinussa, R. M., Dorigo, W. A., & Evans, J. P. (2011). Developing  
706 an improved soil moisture dataset by blending passive and active microwave  
707 satellite-based retrievals. *Hydrol. Earth Syst. Sci.*, 12.
- 708 Liu, Y. Y., van Dijk, A. I. J. M., de Jeu, R. A. M., & Holmes, T. R. H. (2009). An  
709 analysis of spatiotemporal variations of soil and vegetation moisture from a  
710 29-year satellite-derived data set over mainland Australia. *Water Resources*  
711 *Research*, 45(7). doi: 10.1029/2008WR007187
- 712 Lv, L., Liao, K., Lai, X., Zhu, Q., & Zhou, S. (2016). Hillslope soil moisture tempo-  
713 ral stability under two contrasting land use types during different time periods.  
714 *Environmental Earth Sciences*, 75(7), 560. doi: 10.1007/s12665-015-5238-1
- 715 Lv, S., Schalge, B., Saavedra Garfias, P., & Simmer, C. (2020). Required sampling  
716 density of ground-based soil moisture and brightness temperature observations  
717 for calibration and validation of L-band satellite observations based on a vir-  
718 tual reality. *Hydrology and Earth System Sciences*, 24(4), 1957–1973. doi:  
719 10.5194/hess-24-1957-2020
- 720 Machne, R., & Stadler, P. F. (2020). *Piecewise Linear Segmentation by Dynamic*  
721 *Programming*.
- 722 Marañón-Jiménez, S., Radujković, D., Verbruggen, E., Grau, O., Cuntz, M.,  
723 Peñuelas, J., ... Reibmann, C. (2021). Shifts in the Abundances of Sapro-  
724 trophic and Ectomycorrhizal Fungi With Altered Leaf Litter Inputs. *Frontiers*  
725 *in Plant Science*, 12, 682142. doi: 10.3389/fpls.2021.682142
- 726 Maraun, D. (2013). Bias Correction, Quantile Mapping, and Downscaling: Revis-  
727 iting the Inflation Issue. *Journal of Climate*, 26(6), 2137–2143. doi: 10.1175/

- JCLI-D-12-00821.1
- Molero, B., Leroux, D. J., Richaume, P., Kerr, Y. H., Merlin, O., Cosh, M. H., & Bindlish, R. (2018). Multi-Timescale Analysis of the Spatial Representativeness of In Situ Soil Moisture Data within Satellite Footprints: Soil Moisture Time and Spatial Scales. *Journal of Geophysical Research: Atmospheres*, *123*(1), 3–21. doi: 10.1002/2017JD027478
- Pachepsky, Y., & Hill, R. L. (2017). Scale and scaling in soils. *Geoderma*, *287*, 4–30. doi: 10.1016/j.geoderma.2016.08.017
- Pachepsky, Y. A., Guber, A. K., & Jacques, D. (2005). Temporal persistence in vertical distributions of soil moisture contents. *SOIL SCI. SOC. AM. J.*, *69*, 6.
- Pan, F., Pachepsky, Y., Jacques, D., Guber, A., & Hill, R. L. (2012). Data Assimilation with Soil Water Content Sensors and Pedotransfer Functions in Soil Water Flow Modeling. *Soil Science Society of America Journal*, *76*(3), 829–844. doi: 10.2136/sssaj2011.0090
- Peng, Z., Tian, F., Hu, H., Zhao, S., Tie, Q., Sheng, H., . . . Lu, H. (2016). Spatial Variability of Soil Moisture in a Forest Catchment: Temporal Trend and Contributors. *Forests*, *7*(12), 154. doi: 10.3390/f7080154
- Pohl, F., Schrön, M., Rebmann, C., Samaniego, L., & Hildebrandt, A. (2022). *Transforming in situ measurements allows robust estimation of the spatial soil moisture average despite sensor failures: Supporting software code.* Zenodo. doi: 10.5281/zenodo.6669749
- Qin, J., Yang, K., Lu, N., Chen, Y., Zhao, L., & Han, M. (2013). Spatial up-scaling of in-situ soil moisture measurements based on MODIS-derived apparent thermal inertia. *Remote Sensing of Environment*, *138*, 1–9. doi: 10.1016/j.rse.2013.07.003
- Rakovec, O., Samaniego, L., Hari, V., Markonis, Y., Moravec, V., Thober, S., . . . Kumar, R. (2022). The 2018–2020 Multi-Year Drought Sets a New Benchmark in Europe. *Earth's Future*, *10*(3), e2021EF002394. doi: 10.1029/2021EF002394
- Ran, Y., Li, X., Jin, R., Kang, J., & Cosh, M. H. (2017). Strengths and weaknesses of temporal stability analysis for monitoring and estimating grid-mean soil moisture in a high-intensity irrigated agricultural landscape. *Water Resources Research*, *53*(1), 283–301. doi: 10.1002/2015WR018182
- Rebmann, C., Aubinet, M., Schmid, H., Arriga, N., Aurela, M., Burba, G., . . . Franz, D. (2018). ICOS eddy covariance flux-station site setup: A review. *International Agrophysics*, *32*(4), 471–494. doi: 10.1515/intag-2017-0044
- Reichle, R. H. (2004). Bias reduction in short records of satellite soil moisture. *Geophysical Research Letters*, *31*(19), L19501. doi: 10.1029/2004GL020938
- Rivera, D., Lillo, M., & Granda, S. (2014). Representative locations from time series of soil water content using time stability and wavelet analysis. *Environmental Monitoring and Assessment*, *186*(12), 9075–9087. doi: 10.1007/s10661-014-4067-0
- Rolston, D., Biggar, J., & Nightingale, H. (1991). Temporal persistence of spatial soil-water patterns under trickle irrigation. *Irrigation Science*, *12*(4). doi: 10.1007/BF00190521
- Rousseeuw, P. J., & Verboven, S. (2002). Robust estimation in very small samples. *Computational Statistics & Data Analysis*, *40*(4), 741–758. doi: 10.1016/S0167-9473(02)00078-6
- Rowlandson, T., Impera, S., Belanger, J., Berg, A. A., Toth, B., & Magagi, R. (2015). Use of in situ soil moisture network for estimating regional-scale soil moisture during high soil moisture conditions. *Canadian Water Resources Journal / Revue canadienne des ressources hydriques*, *40*(4), 343–351. doi: 10.1080/07011784.2015.1061948
- Samaniego, L., Kumar, R., Thober, S., Rakovec, O., Zink, M., Wanders, N., . . . Attinger, S. (2017). Toward seamless hydrologic predictions across spa-

- 783            tial scales. *Hydrology and Earth System Sciences*, *21*(9), 4323–4346. doi:  
784            10.5194/hess-21-4323-2017
- 785 Schrön, M., Köhli, M., Scheffele, L., Iwema, J., Bogena, H. R., Lv, L., . . . Zacharias,  
786            S. (2017). Improving calibration and validation of cosmic-ray neutron sen-  
787            sors in the light of spatial sensitivity. *Hydrology and Earth System Sciences*,  
788            *21*(10), 5009–5030. doi: 10.5194/hess-21-5009-2017
- 789 Scipal, K., Drusch, M., & Wagner, W. (2008). Assimilation of a ERS scat-  
790            terometer derived soil moisture index in the ECMWF numerical weather  
791            prediction system. *Advances in Water Resources*, *31*(8), 1101–1112. doi:  
792            10.1016/j.advwatres.2008.04.013
- 793 Shao, J., Meng, W., & Sun, G. (2017). Evaluation of missing value imputation  
794            methods for wireless soil datasets. *Personal and Ubiquitous Computing*, *21*(1),  
795            113–123. doi: 10.1007/s00779-016-0978-9
- 796 Singh, G., Panda, R. K., & Mohanty, B. P. (2019). Spatiotemporal Analysis of Soil  
797            Moisture and Optimal Sampling Design for Regional-Scale Soil Moisture Es-  
798            timation in a Tropical Watershed of India. *Water Resources Research*, *55*(3),  
799            2057–2078. doi: 10.1029/2018WR024044
- 800 Thrasher, B., Maurer, E. P., McKellar, C., & Duffy, P. B. (2012). Technical Note:  
801            Bias correcting climate model simulated daily temperature extremes with  
802            quantile mapping. *Hydrology and Earth System Sciences*, *16*(9), 3309–3314.  
803            doi: 10.5194/hess-16-3309-2012
- 804 Tian, J., Han, Z., Bogena, H. R., Huisman, J. A., Montzka, C., Zhang, B., & He,  
805            C. (2020). Estimation of subsurface soil moisture from surface soil moisture  
806            in cold mountainous areas. *Hydrology and Earth System Sciences*, *24*(9),  
807            4659–4674. doi: 10.5194/hess-24-4659-2020
- 808 Vachaud, G., Passerat De Silans, A., Balabanis, P., & Vauclin, M. (1985). Tem-  
809            poral Stability of Spatially Measured Soil Water Probability Density Func-  
810            tion. *Soil Science Society of America Journal*, *49*(4), 822–828. doi:  
811            10.2136/sssaj1985.03615995004900040006x
- 812 van den Burg, G. J. J., & Williams, C. K. I. (2020). An Evaluation of Change Point  
813            Detection Algorithms. *arXiv:2003.06222 [cs, stat]*.
- 814 Vanderlinden, K., Vereecken, H., Hardelauf, H., Herbst, M., Martínez, G., Cosh,  
815            M. H., & Pachepsky, Y. A. (2012). Temporal Stability of Soil Water Contents:  
816            A Review of Data and Analyses. *Vadose Zone Journal*, *11*(4), vzj2011.0178.  
817            doi: 10.2136/vzj2011.0178
- 818 Vereecken, H., Huisman, J., Pachepsky, Y., Montzka, C., van der Kruk, J., Bo-  
819            gena, H., . . . Vanderborght, J. (2014). On the spatio-temporal dynamics  
820            of soil moisture at the field scale. *Journal of Hydrology*, *516*, 76–96. doi:  
821            10.1016/j.jhydrol.2013.11.061
- 822 Vereecken, H., Huisman, J. A., Bogena, H., Vanderborght, J., Vrugt, J. A., &  
823            Hopmans, J. W. (2008). On the value of soil moisture measurements in  
824            vadose zone hydrology: A review. *Water Resources Research*, *44*(4). doi:  
825            10.1029/2008WR006829
- 826 Wang, C., Fu, B., Zhang, L., & Xu, Z. (2019). Soil moisture–plant interactions: An  
827            ecohydrological review. *Journal of Soils and Sediments*, *19*(1), 1–9. doi: 10  
828            .1007/s11368-018-2167-0
- 829 Wang, C., Zuo, Q., & Zhang, R. (2008). Estimating the necessary sampling size of  
830            surface soil moisture at different scales using a random combination method.  
831            *Journal of Hydrology*, *352*(3-4), 309–321. doi: 10.1016/j.jhydrol.2008.01.011
- 832 Wang, J., Ge, Y., Heuvelink, G., & Zhou, C. (2015). Upscaling In Situ Soil Mois-  
833            ture Observations to Pixel Averages with Spatio-Temporal Geostatistics. *Re-  
834            mote Sensing*, *7*(9), 11372–11388. doi: 10.3390/rs70911372
- 835 Wang, S., Shan, H., Zhang, C., Wang, Y., & Shi, C. (2018). Bias Correction in  
836            Monthly Records of Satellite Soil Moisture Using Nonuniform CDFs. *Advances  
837            in Meteorology*, *2018*, 1–11. doi: 10.1155/2018/1908570

- 838 Wang, T., Wedin, D. A., Franz, T. E., & Hiller, J. (2015). Effect of vegetation on  
839 the temporal stability of soil moisture in grass-stabilized semi-arid sand dunes.  
840 *Journal of Hydrology*, *521*, 447–459. doi: 10.1016/j.jhydrol.2014.12.037
- 841 Wei, L., Dong, J., Gao, M., & Chen, X. (2017). Factors Controlling Temporal Stabili-  
842 ty of Surface Soil Moisture: A Watershed-Scale Modeling Study. *Vadose Zone*  
843 *Journal*, *16*(10), vzj2016.12.0132. doi: 10.2136/vzj2016.12.0132
- 844 Wollschläger, U., Attinger, S., Borchardt, D., Brauns, M., Cuntz, M., Dietrich, P.,  
845 ... Zacharias, S. (2017). The Bode hydrological observatory: A platform for  
846 integrated, interdisciplinary hydro-ecological research within the TERENO  
847 Harz/Central German Lowland Observatory. *Environmental Earth Sciences*,  
848 *76*(1), 29. doi: 10.1007/s12665-016-6327-5
- 849 Xu, S., & Cheng, J. (2021). A new land surface temperature fusion strategy  
850 based on cumulative distribution function matching and multiresolution  
851 Kalman filtering. *Remote Sensing of Environment*, *254*, 112256. doi:  
852 10.1016/j.rse.2020.112256
- 853 Yao, P., Lu, H., Shi, J., Zhao, T., Yang, K., Cosh, M. H., ... Entekhabi, D.  
854 (2021). A long term global daily soil moisture dataset derived from  
855 AMSR-E and AMSR2 (2002–2019). *Scientific Data*, *8*(1), 143. doi:  
856 10.1038/s41597-021-00925-8
- 857 Zanella, P. G., de Carvalho, C. A. B., Ribeiro, E. T., Madeiro, A. S., & Gomes,  
858 R. D. S. (2017). Optimal quadrat area and sample size to estimate the  
859 forage mass of stargrass. *Semina: Ciências Agrárias*, *38*(5), 3165. doi:  
860 10.5433/1679-0359.2017v38n5p3165
- 861 Zappa, L., Forkel, M., Xaver, A., & Dorigo, W. (2019). Deriving Field Scale Soil  
862 Moisture from Satellite Observations and Ground Measurements in a Hilly  
863 Agricultural Region. *Remote Sensing*, *11*(22), 2596. doi: 10.3390/rs11222596
- 864 Zhang, D., Zhang, W., Huang, W., Hong, Z., & Meng, L. (2017). Upscaling of Sur-  
865 face Soil Moisture Using a Deep Learning Model with VIIRS RDR. *ISPRS In-*  
866 *ternational Journal of Geo-Information*, *6*(5), 130. doi: 10.3390/ijgi6050130
- 867 Zhao, Y., Peth, S., Wang, X. Y., Lin, H., & Horn, R. (2010). Controls of surface soil  
868 moisture spatial patterns and their temporal stability in a semi-arid steppe.  
869 *Hydrological Processes*, *24*(18), 2507–2519. doi: 10.1002/hyp.7665
- 870 Zhu, X., He, Z., Du, J., Chen, L., Lin, P., & Tian, Q. (2021). Spatial heterogeneity  
871 of throughfall and its contributions to the variability in near-surface soil water-  
872 content in semiarid mountains of China. *Forest Ecology and Management*, *488*,  
873 119008. doi: 10.1016/j.foreco.2021.119008
- 874 Zhu, X., Shao, M., & Liang, Y. (2018). Spatiotemporal characteristics and  
875 temporal stability of soil water in an alpine meadow on the northern Ti-  
876 betan Plateau. *Canadian Journal of Soil Science*, CJSS-2017-0078. doi:  
877 10.1139/CJSS-2017-0078
- 878 Zhuang, R., Zeng, Y., Manfreda, S., & Su, Z. (2020). Quantifying Long-Term Land  
879 Surface and Root Zone Soil Moisture over Tibetan Plateau. *Remote Sensing*,  
880 *12*(3), 509. doi: 10.3390/rs12030509